Cardiovasc Intervent Radiol (2019) 42:893–904
https://doi.org/10.1007/s00270-019-02182-0

LABORATORY INVESTIGATION

The Role of a Curved Electrode with Controllable Direction in the Radiofrequency Ablation of Liver Tumors Behind Large Vessels

An-Na Jiang[1] · Song Wang[1] · Wei Yang[1] · Kun Zhao[1] · Xiu-Mei Bai[1] · Zhong-Yi Zhang[1] · Wei Wu[1] · Min-Hua Chen[1] · Kun Yan[1]

Received: 8 November 2018 / Accepted: 5 February 2019 / Published online: 13 February 2019

Abstract

Purpose To investigate the role of a novel curved radiofrequency ablation (RFA) electrode with controllable direction in the ablation of tumors behind large hepatic vessels in ex vivo bovine and in vivo canine liver experiments.

Materials and Methods Approval from the institutional animal care and use committee was obtained. In ex vivo experiments, conventional multi-tines expandable electrodes, conventional monopolar straight electrodes and novel curved electrodes were used in the ablation of the bovine liver ($n = 90$). The ablated area, parallel axis, vertical axis and shape of different electrodes were compared. Then, 24 beagle dogs (10 months old, female) were used for in vivo experiments. Visual tumor targets deeply located in the portal vein were established, and ultrasound-guided liver ablation was performed with different electrodes. The ablation range, target coverage rate, percentage of normal tissue injury and damage to adjacent vessels were evaluated. The Kruskal–Wallis test and the Chi-squared test were used for statistical analysis.

Results For the ex vivo study with a 3-cm electrode, the ablation area of the multi-tines expandable electrode group (7.14 ± 0.16 cm^2) was significantly larger than that of the novel curved electrode group (5.01 ± 0.30 cm^2, $P < 0.001$) and the monopolar straight electrode group (5.43 ± 0.15 cm^2, $P < 0.001$). The results obtained with the 4-cm electrode in the three groups were in accordance with those of the 3-cm electrode. In vivo, the normal tissue damage area of the novel curved electrode group was smaller than that of the multi-tines expandable electrode group (1.10 ± 0.18 cm^2 vs. 4.00 ± 0.18 cm^2, $P < 0.001$). The target coverage rate of the novel curved electrode group was better than that of the monopolar straight electrode group (100% vs. $80.86 \pm 1.68\%$, $P < 0.001$). The hematoxylin and eosin (H&E) and TUNEL staining results showed that the ablation necrosis area was adjacent to large vessels, but the vascular wall was not significantly damaged in the novel curved electrode group.

Conclusion Our preliminary results showed that the novel curved RFA electrode with controllable direction could achieve accurate ablation for tumors behind large hepatic vessels, with a better target coverage rate and less damage to normal tissue, than conventional multi-tines expandable electrodes and monopolar straight electrodes.

Keywords Radiofrequency ablation · Electrode · Controllable direction · Hepatic vessel · Target coverage rate

An-Na Jiang and Song Wang, these two authors contributed equally to this work.

Electronic supplementary material The online version of this article (https://doi.org/10.1007/s00270-019-02182-0) contains supplementary material, which is available to authorized users.

✉ Wei Yang
13681408183@163.com

[1] Department of Ultrasound, Key Laboratory of Carcinogenesis and Translational Research (Ministry of Education/Beijing), Peking University Cancer Hospital and Institute, 52 Fucheng Road, Haidian District, Beijing 100142, China

Introduction

Radiofrequency ablation (RFA) is one of the most widely used techniques in tumor ablation. During RFA, the electrode needle is directly punctured into tumor tissue under the guidance of ultrasound or computed tomography (CT) imaging [1, 2]. The RFA electrode needle can be heated to a high temperature exceeding 80 °C, resulting in cell death to generate a coagulative necrosis area in the tumor site [3, 4]. The electrode is a core component of RFA instruments because it directly affects the size and shape of the coagulative necrosis area.

The conventional RFA electrodes include two main types. One type is a single-needle straight electrode consisting of monopolar (e.g., TYCO Healthcare, USA) and bipolar electrodes (e.g., CELON Lab Power, Germany), the other type is a multi-tines expandable electrode (e.g., RITA Medical System, USA) [5, 6], as shown in Figure S1. Using the single-needle straight electrode, the insertion made along a straight pathway, and one or more electrode needles are simultaneously inserted into the lesions for ablation [7]. However, when a tumor is located at a deep site of a blood vessel, crossing the single-needle straight electrode over a great vessel to ablate the tumor located behind it is difficult, and it is also easy to puncture the blood vessel and increase the incidence of hemorrhagic complications. The second type of conventional RFA electrode is a multi-tines expandable electrode comprising 8–10 bendable arc-shaped tines located inside a trocar. All tines are uniformly distributed in 360° by one operation of needle arrangement and can produce spherical and reproducible necrotic lesions [8, 9]. However, when the tumor is located at the deep site of a great vessel, the electrode needles cannot access the center of the tumor to completely cover the whole tumor while avoiding the vessel, which results in the incomplete ablation of the tumor or causes damage to the vessels and normal tissue [10].

Thus, the existing RFA electrodes (Fig. 1A, B) fail to perform an oriented ablation to fit the tumors in complicated anatomic locations in the liver. In view of the above-mentioned problems in the tumor ablation field, we invented a novel curved RFA electrode with controllable direction by combining design elements from related manufacturing fields with years of user experience to overcome the drawbacks mentioned above (Fig. 1C). In this study, we aimed to evaluate the feasibility, efficiency and safety of the novel RFA electrode in the ablation of tumors located behind great vessels in ex vivo and in vivo animal experiments.

Methods and Materials

Design of the RFA Electrode

In our design of the novel RFA electrode (Fig. 2A), a plurality of control sliding blocks is uniformly arranged circumferentially in the handle portion, and each tine is individually controlled by one sliding block to implement independent extension or retraction to control the extension number and the direction and length of the tines; overcome the defect of traditional electrodes for which the number and the extending direction of the tines are invariable; realize a controlled and oriented expansion of the electrode tines; achieve an accurate ablation; prevent unnecessary damage and obtain the advantages of strong targeting ability, good local effect, low complications, flexible operation and ease of adjustment.

According to our design, we modified existing 15 G multi-tines expandable RFA electrodes with 3 cm and 4 cm curved tines (Medsphere, International Company) as prototype novel electrodes in this study. The electrode array consists of five expanded stainless-steel tines held in place by a trocar that is 0°–180° (45° between two tines), allowing the user to adjust the direction of tines expansion as desired (Fig. 2B). The tines of the electrodes in this study have two angulations, 30° and 45° for the 3-cm and 4-cm electrodes, respectively. For the 3-cm electrode, each tine can be exposed as far as 1.5 cm, and for the 4-cm electrode, each tine can be exposed as far as 2 cm. The tines can be activated simultaneously and individually. Conventional multi-tines expandable electrodes (Medsphere, international company) and monopolar straight electrodes (Medsphere, International Company) were used as controls in this study since both types of electrodes are commercially available. Thus, we can compare the novel electrode and the conventional two electrodes with the same generator and the same operation parameters. The electrodes with 3 cm and 4 cm tines were adopted in the ex vivo experiment, and the 4-cm tines electrode was used in the in vivo experiment. The tines of the electrode were fully exposed during every ablation.

Ex Vivo Experiments

In total, 90 ablations were performed on freshly excised, room-temperature bovine livers placed on a grounding pad (Thermopad; RITA/Angiodynamics) in a medical tray. The electrode tips were advanced with great caution at least 4 cm into the target tissue to ensure that no active tip was exposed in the air. The electrode was inserted with a minimum of 5 cm between each insertion point to avoid interactions between each ablation. The morphology and

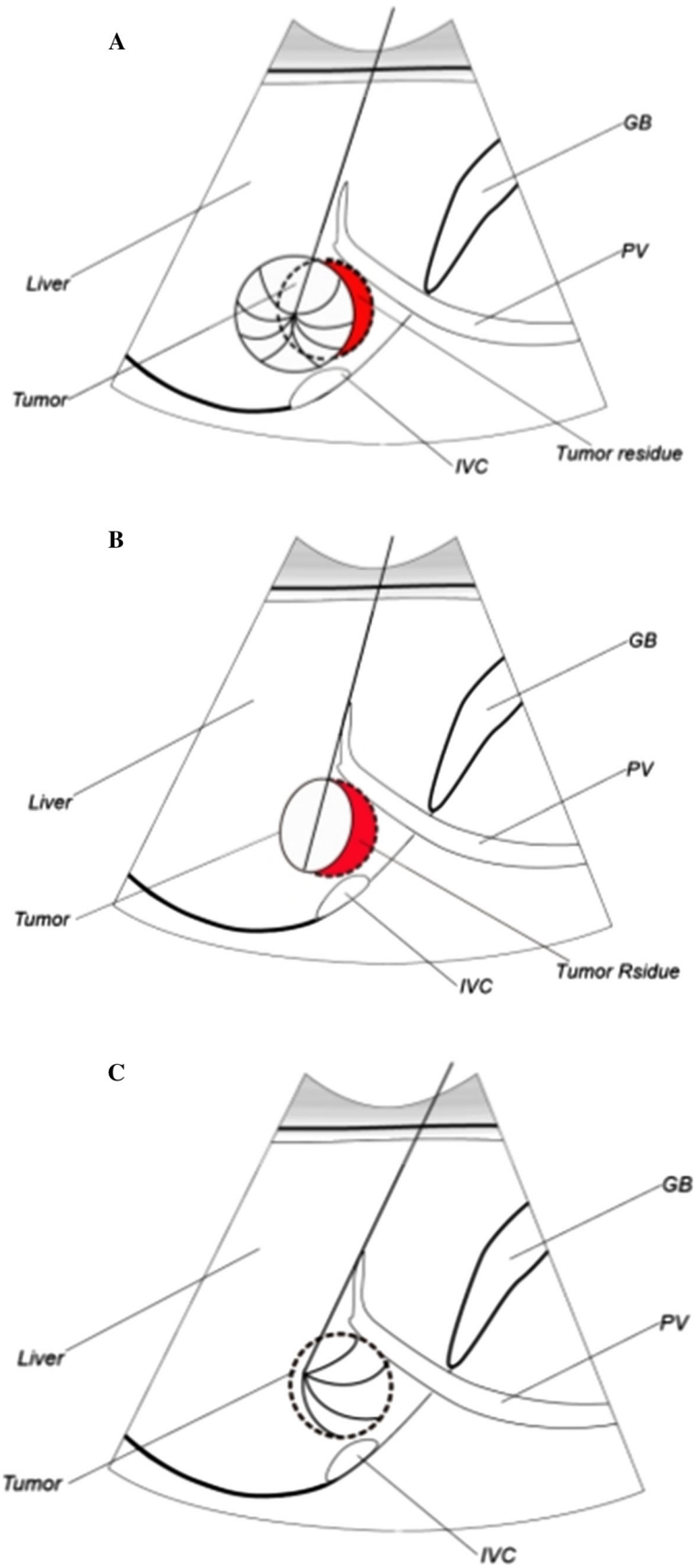

Fig. 1 A schematic diagram of the problems of conventional radiofrequency ablation electrodes and the advantage of a novel curved radiofrequency ablation electrode for treating liver tumors behind large vessels. **A** Multi-tines expandable electrode. **B** Monopolar straight electrode. **C** Novel curved electrode

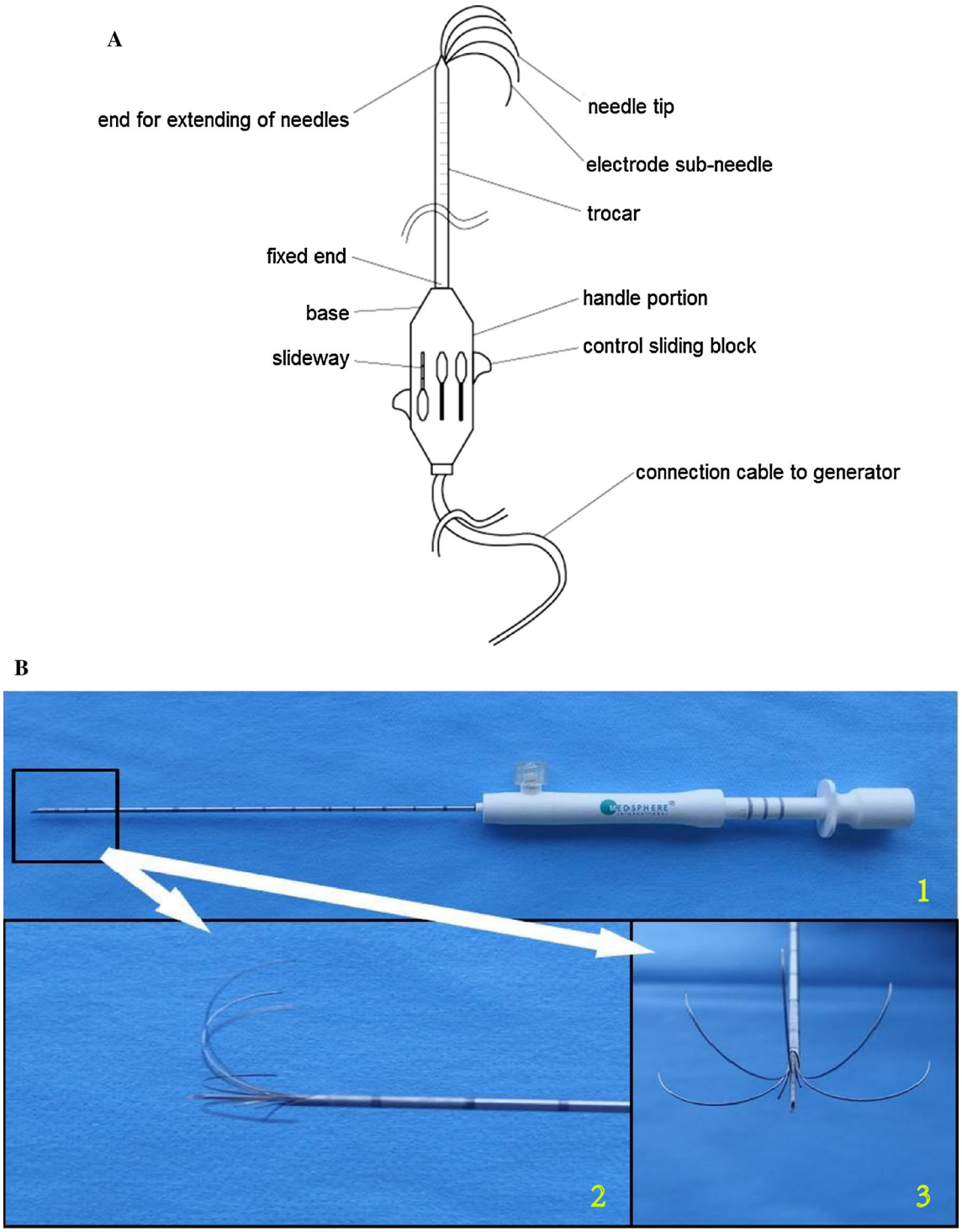

Fig. 2 The new radiofrequency ablation electrode—which we named the novel curved controlled direction radiofrequency ablation electrode. **A** A schematic diagram of the novel radiofrequency ablation electrode. **B** Photograph of the novel curved radiofrequency ablation electrode (we modified the existing multi-tines expandable electrode) used in this study. **B-1**. The overview of the electrode. **B-2**. The top review for the needle tip of the electrode. **B-3**. The front review of the needle tip of the electrode

echogenicity in ultrasound imaging for each group during ablation were recorded and compared. The shape of coagulation, vertical diameter and parallel diameter, as well as the ablation area, were evaluated at 120 min after RFA in gross pathological samples [11]. The ex vivo experimental ablations were performed by two authors with more than 3 and 5 years of experience in animal experiments (J.A.N. and W.S., respectively).

Assessment of the Ablation Zone

The liver-containing lesions were dissected on the parallel plane to the axis of the electrode insertion. The clear gray area corresponds to the zone of coagulation necrosis [12, 13]. The same two authors (J.A.N. and W.S.) used calipers to measure the vertical diameter (Dv) and the parallel diameter (Dp) of the white region on the slice to show its maximum area. The range of the ablation zone was drawn by hand and auto calculated by imaging analysis software (ImageJ v. 1.42, National Institutes of Health, Bethesda, MD) [14] (Figure S2). To compare the configuration of the ablation zones in each group, the ratio of Dv to Dp was also calculated.

In Vivo Confirmation

For in vivo experiments, we chose a canine liver model because canine livers have multiple large vessels that mimic human liver vascularity. Twenty-four female beagle dogs (10 months old, 20 kg) were purchased from HFK Bioscience Co., Ltd. (Beijing, China), and all procedures were approved by the institutional animal care and use committee. The animals were anesthetized via the intravenous injection of 3% sodium pentobarbital (30 mg/kg, Chemical Reagent Factory, Foshan, China). The dogs were placed in a supine position, prepared at the midline and draped. A standardized grounding pad was attached to the back to complete an electrical circuit. The 24 animals were randomized into three groups (eight animals in each group) to undergo RFA under a-portal vein (< 5 mm in distance) with the above three electrodes. Each ablation was only conducted for one dog to assess the hemorrhage risk after ablation. Ultrasound was used to detect the large portal vein in the right lobe of the liver, guiding electrode placement and monitoring the ablation procedure. Intraperitoneal bleeding was considered if increased liquid in front of the liver was detected by ultrasound. The short-axis cross section of the portal vein was set as the electrode placement section. Liver tissue (3 cm in diameter) directly under the portal vein was proposed as the target area. In all three groups, the electrode was inserted at 45° vertical to the liver surface, and the portal vein was crossed to place the electrode in the target area. The morphology, echogenicity and range of ultrasound imaging for each group during ablation were recorded and compared. The pathological changes, ablation necrosis range, target effect, damage to normal liver tissue and hemorrhage rate for each group were compared. In this phase, ablations were performed by one senior author with more than 10 years of experience in interventional ultrasound (Y.W.).

RFA Procedure

The electrodes in all three groups were applied by using a 480-kHz RFA generator (Medsphere S-1500). During ablation, the radiofrequency generator was started at a 30 W output. The output increase was sufficient to maintain a tip temperature of 80–100 °C until the resistance reached 100 Omega. When the tip temperature reached the designated temperature (120 °C), the generator stopped automatically. Ablation time was determined automatically by the radiofrequency energy generator. All tines of the RFA electrode were fully exposed during ablation. In addition, tract coagulation was performed in all animals.

Evaluation of Pathological Changes and Target Effect

At 24 h after ablation, the animals were euthanized by an intracardial injection of potassium chloride (Shanghai Haoran Biological Technology Co., LTD, Shanghai, China). A diagnostic inspection of the abdominal cavity of each dog was performed to assess postoperative bleeding. After removal, livers containing RF-induced coagulations were sliced in parallel to the electrode tracks. The liver and vessels in the ablation range were resected and evaluated. We incubated one slice of each section in 2% 2,3,5-triphenyltetrazolium chloride (TTC) (Sigma-Aldrich, St Louis, MO), which indicates mitochondrial enzyme activity, at 37 °C for 30 min to assess the irreversible cellular injury of RF-induced necrosis [15, 16]. Area analysis was performed on the photographs using ImageJ v. 1.42 software (National Institutes of Health, Bethesda, MD). The target area was set to simulate the tumor located behind the portal vein in each dog. The target area was a circular region with a 3 cm diameter located directly behind the portal vein, imitating a small tumor, as shown in Fig. 3. The ablation area, the

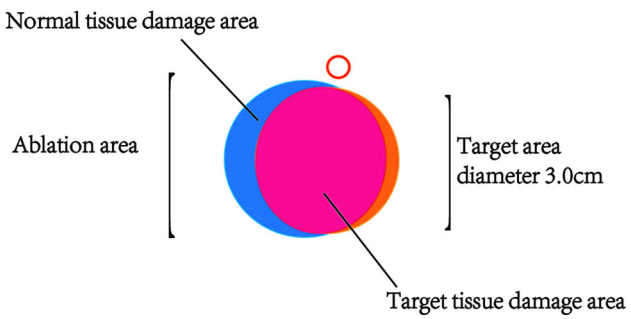

Fig. 3 A schematic diagram of the vessel, ablation and target area calculation. The red hollow circle represents the vessel, the blue circle represents the ablation area, and the yellow circle represents a target area of 3 cm in diameter. The overlapped pink area represents the target tissue damage area

target coverage rate and the percentage of normal tissue injury were calculated after ablation.

After photography, the rest of the resected liver samples were fixed in 10% formalin solution for subsequent histopathologic examination. The pathological findings of the ablation zone were evaluated by H&E staining. The damage to the vascular wall or normal liver tissues near the ablation was recorded by H&E staining and TUNEL staining.

Statistical Analysis

Statistical analysis was performed using SPSS 21.0 (SPSS, Chicago, IL, USA). All continuous data are shown as the mean ± standard deviation. The Kruskal–Wallis test was used to compare the ablation size among the three groups. Then, the Nemenyi test was used to perform paired comparisons for multiple groups when the overall P value was less than 0.05. The prevalence of bleeding was compared using a Chi-squared test and Fisher's exact test. A P value of less than 0.05 was considered significant.

Results

Ex Vivo Experiments

The Ultrasound Image Findings

A strong hyperechoic region was produced around the electrode needle after starting the RFA generator. The region was round in the multi-tines expandable electrode group, semilunar-shaped in the novel curved electrode group and oval-shaped in the monopolar straight electrode group. The boundary of the strong echo region was well defined, and the echogenicity was uniform (Fig. 4).

The Morphology and Range of the Ablative Zone on Pathological Samples

The shape of the ablative zone on the gross pathological specimen was in accordance with the ultrasound presentation. The gross pathological specimen showed that the ablative necrosis region was nearly round in the multi-tines expandable electrode group, was semilunar in the novel curved electrode group and oval-shaped in the monopolar straight electrode group (Fig. 4).

The range of the gross pathological ablation area was measured by using calipers and imaging software (Table 1). With a 3-cm electrode, the ablation Dv of the multi-tines expandable electrode group (3.50 ± 0.35 cm) was significantly longer than the novel curved electrode group (2.37 ± 0.23 cm, $P = 0.001$) and the monopolar straight electrode group (2.12 ± 0.06 cm, $P = 0.001$). The ablation Dp of the monopolar straight electrode group (3.53 ± 0.06 cm) was significantly longer than those of the multi-tines expandable electrode group (3.10 ± 0.10 cm, $P = 0.008$) and the novel curved electrode group (2.57 ± 0.21 cm, $P < 0.001$). The ablation area of the multi-tines expandable electrode group (7.14 ± 0.16 cm^2) was significantly larger than that of the novel curved electrode group (5.01 ± 0.30 cm^2, $P < 0.001$) and monopolar straight electrode group (5.43 ± 0.15 cm^2, $P < 0.001$) (Figure S3). The results obtained with the 4-cm electrode in the three groups were in accordance with those of the 3-cm electrode (Table 1).

In Vivo Confirmation

The Ultrasound Findings and Target Effect

Similar to the ex vivo results, there was a strong hyperechoic area around the electrode during ablation, the boundary was well defined and the echogenicity was uniform. The shape of the multi-tines expandable electrode group was round, the novel curved electrode group was demilunar and the monopolar straight electrode group was oval-shaped. The ablative area was located behind the large portal vein in the liver (Fig. 5).

Based on ultrasound findings, the target effect for different electrodes was as follows: the target area was completely covered, while a large portion of normal liver was damaged in the multi-tines expandable electrode group; the target area was completely covered, and slight normal liver damage was observed in the novel curved electrode group. The target area was partially covered by ablation in the monopolar straight electrode group.

Pathological Evaluation of the Ablation Zone and Target Effect

According to gross pathological evaluation of the ablation zone in the liver, the necrosis zone was brown and yellow, the narrow needle path was slightly black in the center, and the edge color was gradually dimmed. Histopathologic findings confirmed that the ablated regions in all cases consisted of a central necrotic zone surrounded by a 1–3-mm-wide, peripheral hemorrhagic zone consisting of necrotic hepatocytes, interstitial hemorrhage and polymorphonuclear leukocyte infiltrates. There was a sharp demarcation between coagulated and untreated tissue. The ablated region was nearly round in the multi-tines expandable electrode group, demilunar in the novel curved electrode group and a long oval-shaped in the monopolar straight electrode group. These features were consistent with the ex vivo results (Fig. 5).

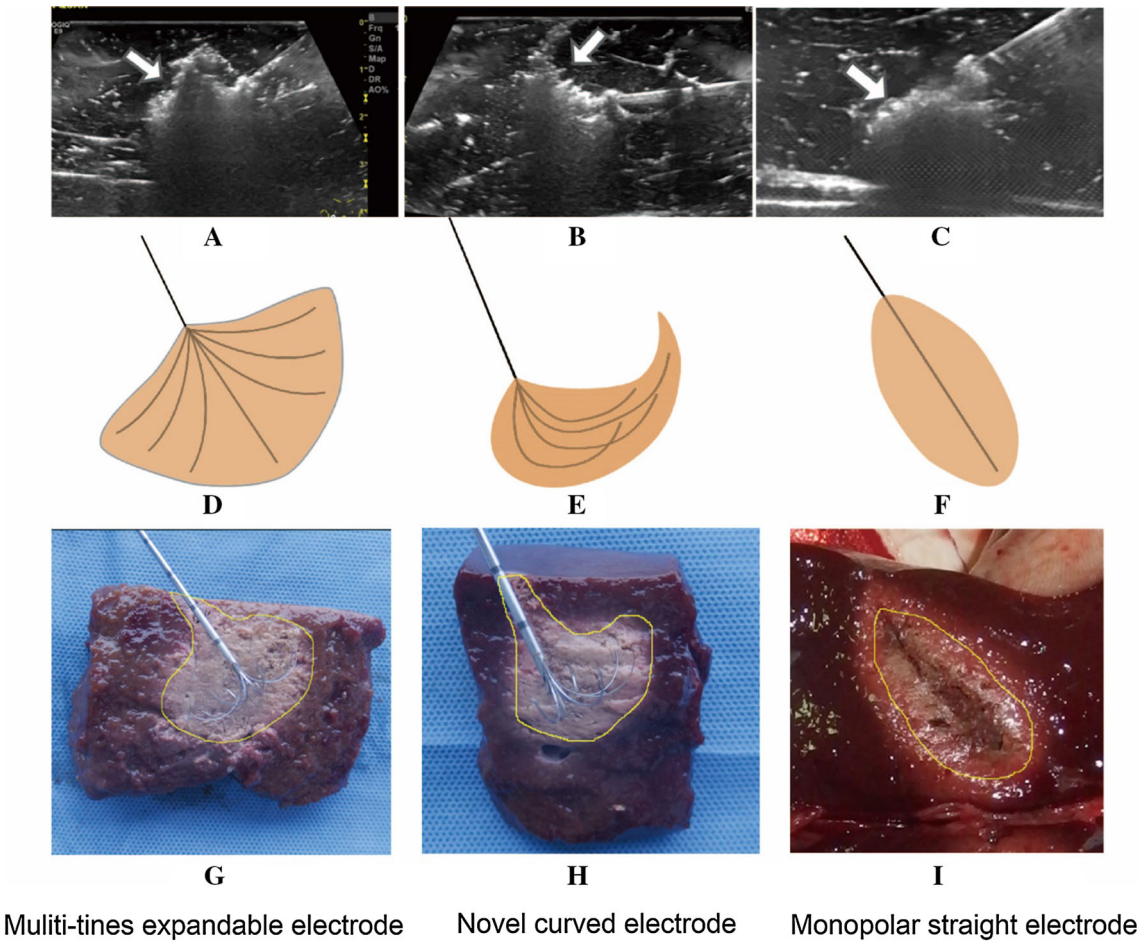

Fig. 4 The texture and morphology of the ablation zone in ultrasound imaging and gross pathology with different electrodes in ex vivo experiments (bovine liver). **A–C** The ultrasound performance of different RFA electrodes in ex vivo experiments. **D–F** Schematic of the ablation zone with different electrodes. **G–I** The corresponding finding in gross pathological samples with different electrodes

Table 1 Comparison of the ablation range on gross samples among different electrodes

Measurement	Dp (cm)	Dv (cm)	Area (cm^2)	Ratio of Dp/Dv
Multi-tines expandable				
3 cm	3.10 ± 0.10	3.50 ± 0.35	7.14 ± 0.16	0.89 ± 0.06
4 cm	3.37 ± 0.12	5.10 ± 0.53	12.43 ± 0.33	0.66 ± 0.07
Novel curved				
3 cm	2.57 ± 0.21	2.37 ± 0.23	5.01 ± 0.30	1.10 ± 0.20
4 cm	2.80 ± 0.10	3.00 ± 0.20	8.05 ± 0.81	0.84 ± 0.05
Monopolar straight				
3 cm	3.53 ± 0.06	2.12 ± 0.06	5.43 ± 0.15	1.63 ± 0.04
4 cm	5.13 ± 0.23	2.27 ± 0.25	9.97 ± 0.06	2.28 ± 0.19

The ablations Dp, Dv and area were significantly different among three groups in both the 3-cm electrode and the 4-cm electrode. The ratio of Dp/Dv indicated the morphology of the ablation zone. The more the ratio was close to 1, the more the shape was close to a circle

Based on pathological gross samples, the ablation area was 11.13 ± 0.19 cm^2 for the multi-tines expandable electrode, 8.73 ± 0.26 cm^2 for the novel curved electrode, and 9.34 ± 1.07 cm^2 for the monopolar straight electrode (Table 2). We further compared the target coverage area and normal tissue damage area, and found that the target coverage area was smallest in the monopolar straight group (5.73 ± 0.13 cm^2, $P < 0.001$, $P < 0.001$), while the

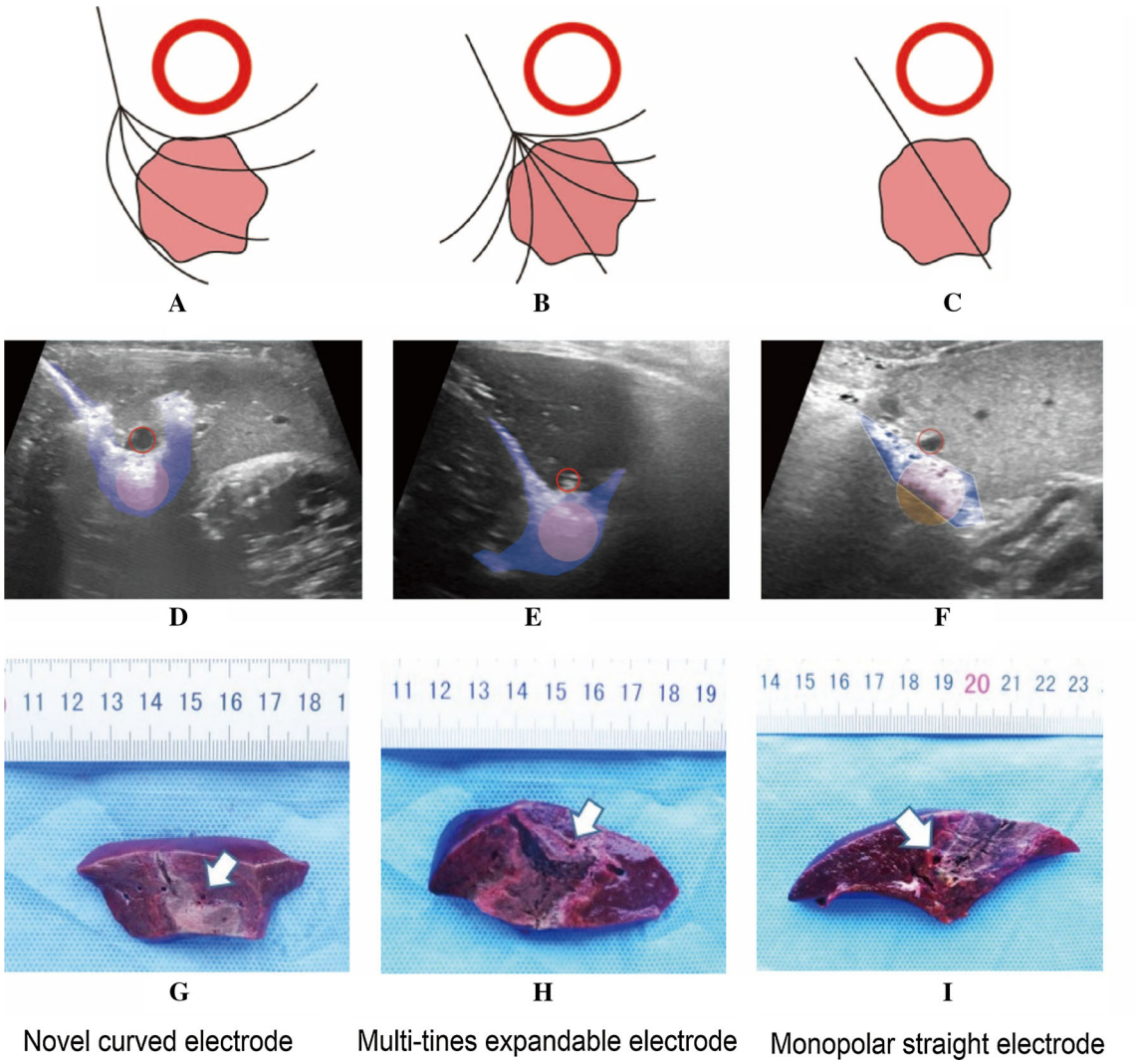

Fig. 5 The morphology and size of the ablation zone in ultrasound imaging and gross pathology with different electrodes in the in vivo experiments (beagle dogs). **A–C** Scheme of the ablation zone with different electrodes. **D–F** The ultrasound performance of different RFA electrodes in vivo. The red hollow circle represents the vessel, the blue area indicates the ablation area, and the pink area indicates the target tissue damage area. **G–I** The corresponding finding in gross pathological samples with different electrodes. The arrow points to the vessel

Table 2 Comparison of the ablation area and target coverage rate for different electrodes

Parameters	Multi-tines	Novel	Monopolar
Target tissue area* (cm^2)	7.1	7.1	7.1
Target tissue damage area (cm^2)	7.1	7.1	5.73 ± 0.13
Target coverage rate (%)	100	100	80.86 ± 1.68
Ablation area (cm^2)	11.13 ± 0.19	8.73 ± 0.26	9.34 ± 1.07
Normal tissue damage area** (cm^2)	4.00 ± 0.18	1.10 ± 0.18	3.49 ± 0.74
Normal tissue damage ratio** (%)	36.20 ± 1.18	12.56 ± 2.01	37.75 ± 8.26

*The target tissue area of each group was set equal. 7.1 cm^2 is the area of the circle of 3 cm in diameter according to formula ($S = \pi r^2$)

**The normal tissue damage area and damage ratio were significantly different among the three groups ($P < 0.001$)

normal tissue damage area was largest in the multi-tines expandable electrode group (4.00 ± 0.18 cm^2, $P < 0.001$, $P = 0.002$) compared to that in the other two groups. The target coverage rate of the novel curved electrode was better than that of the monopolar straight electrode (100% vs. 80.68 ± 1.68%, $P < 0.001$). Additionally, the normal tissue damage rate of the novel curved electrode was better than that of the multi-tines expandable electrode (12.56 ± 2.01% vs. 36.2 ± 1.18%, $P < 0.001$) (Table 2).

Pathological Evaluation of the Vessels Above the Ablation Zone

The H&E and TUNEL staining results of the ablation sample showed that the ablation necrosis area was adjacent to the vessel, but the vascular wall was not significantly damaged in the novel curved electrode group. However, the vascular wall was obviously destroyed in the monopolar straight electrode group and was mildly damaged in the multi-tines expandable group (Fig. 6).

Complications

After RFA treatment, the rate of peritoneal bleeding was 25% (2/8 ablations) in the multi-tines expandable electrode group and 75% (6/8 ablations) in the monopolar straight electrode group, while there was no obvious bleeding in the novel curved electrode group ($P = 0.005$ for overall comparison). There was a thrombus near the multi-tines expandable electrode needle insertion. The risk of bleeding after RFA in the novel curved electrode group was significantly lower than that in the monopolar straight electrode group ($P = 0.007$).

Discussion

RFA is a safe and effective minimally invasive therapy widely used in unresectable hepatic tumors. RFA can be used as a radical therapy in tumors under 3 cm and has important effects in alleviating tumor load and prolonging survival in the treatment of large tumors [17–21]. In recent years, the effectiveness of RFA has obtained increasing approval and satisfaction, and relevant research has also attracted great attention as a minimally invasive therapy. Most research has focused on expanding the ablation zone for better effects, such as optimizing the RF algorithm [22–24], increasing the tip of the electrode needle [25–27] and combining this technique with other therapies such as transcatheter arterial chemoembolization [28–30]. However, the extent of coagulation for some of the newer electrode systems damages adjacent tissue because the liver has complex anatomic structures. The ablation size was larger, and the risk for injury of adjacent structures and

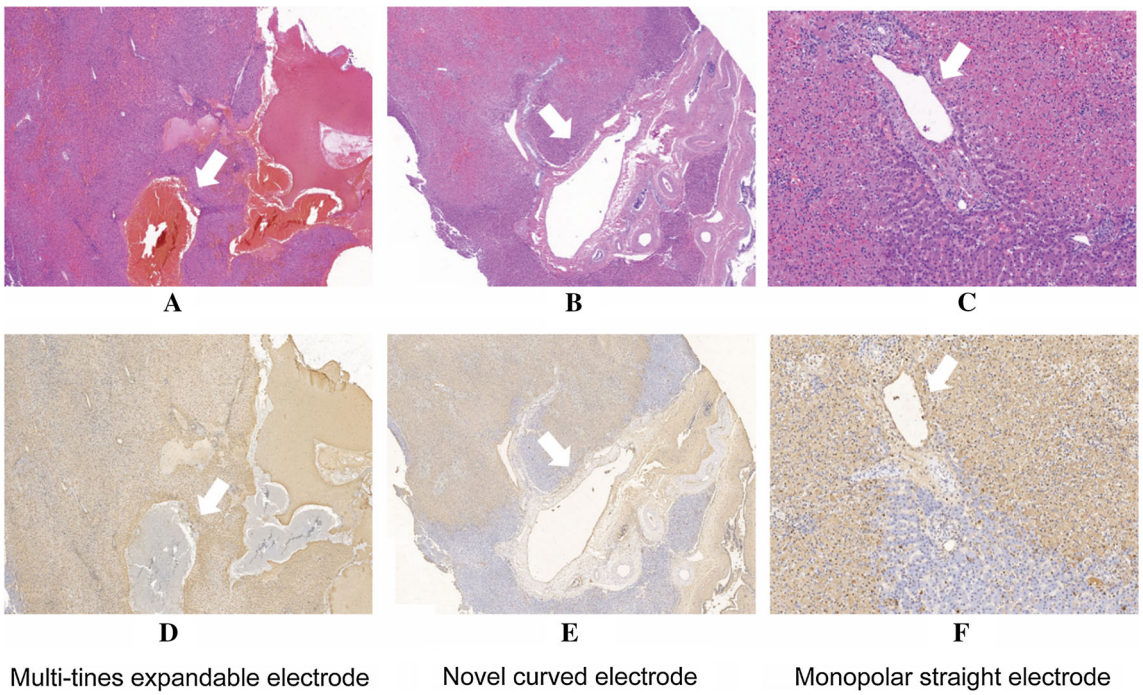

Fig. 6 Pathological staining results for the liver with vessels from in vivo experiments (beagle dogs). Hematoxylin and eosin (**A**–**C**) and TUNEL (**D**–**F**) staining showed that the nonviable treated tissue was alongside the vessel. The thrombus can be observed in the multi-tines expandable electrode group. The vascular wall was also damaged in the monopolar straight group. The vascular wall cells were still well formed in the novel curved electrode group. The arrow points to the vessel

resulting complications was higher. Thus, the ablation accuracy had a direct impact on the treatment efficiency. However, this kind of research has focused on the improving image guidance methods [31], and to our knowledge, very few researchers have focused on modifying the RFA electrode.

RFA of hepatic tumors is often hindered by their location close to the major hepatic vessels. In the past, RFA for perivascular tumors was thought to be ineffective and unsafe due to either the heat sink effect or vascular thrombosis [32–35]. Specifically, it is difficult for tumors located just behind major vessels because of the limit of the puncture angle of the electrode during the percutaneous RFA procedure. To address this limitation, we developed a RFA electrode capable of thermally coagulating a typical shape to cross large vessels and target the tumors located behind these structures, without touching the vessels. The aim of this study was to examine whether RFA using a novel curved electrode could be a safe and effective option for targeting tumors behind major hepatic vessels.

Our results revealed that the novel curved electrode with a controllable direction could cover the target area and minimize the damage of the normal tissue in the ablation behind hepatic vessels in an animal model. This method was able to create coagulations of a circle larger than 3 cm in diameter in the in vivo liver tissue, which was large enough to safely treat tumors under 3 cm.

Regarding the ablation size with different electrodes in ex vivo experiments, the number of extended tines of the novel curved electrode was less than that of the multi-tines expandable electrode; thus, the Dv of the novel curved electrode was shorter than that of the multi-tines expandable electrode (2.37 ± 0.23 cm vs. 3.50 ± 0.35 cm, $P = 0.001$). Accordingly, the ablation area was also smaller (5.01 ± 0.30 cm^2 vs. 7.14 ± 0.16 cm^2, $P = 0.000$). Hence, the novel curved electrode could only cover the tumor range while reducing normal tissue injury, especially adjacent organs, such as large vessels. Compared to the monopolar straight electrode, the ablation area of the novel curved electrode was similar (5.01 ± 0.30 cm^2 vs. 5.43 ± 0.15 cm^2, $P = 0.352$). However, the shape of the ablation zone was quite different. The ablation zone of the novel curved electrode was semilunar, which better fit the tumor under the vessel. Therefore, compared with the monopolar straight electrode, the novel curved electrode could be better able to cover the tumor and reduce residue tissue. The 3-cm and 4-cm electrodes are most commonly used in clinical treatment, so we chose these two electrodes for this experiment. The comparison among the three groups with different electrodes was consistent between the 3-cm and 4-cm electrodes. Notably, the ablation size in ex vivo experiments was usually larger than that in vivo experiments. We believe that the lack of blood flow and perfusion may lead to the overestimation of the achievable ablation zone in an ex vivo study.

In the in vivo experiments, we set a virtual tumor (3 cm in diameter) in the deep site of the vessel. We evaluated the target coverage rate on the largest transverse section of pathological sample and ultrasound images, so the target coverage rate of the multi-tines electrode was 100%. However, in clinical practice, the tumor was spherical, and it was usually difficult to fully ablate the whole tumor without damaging the vessels located above the tumor. When comparing the bleeding post-ablation, the novel curved electrode had the lowest risk compared with that of the other two groups ($P = 0.005$). The pathological staining analysis indicated coagulative necrosis, and the demarcation between treated and untreated tissue could be identified. Complete cell necrosis was observed surrounding the vessel within the ablation zone, while the vascular wall cells remained viable in the novel curved electrode group. However, membrane rupture and pyknosis indicated irreversible necrosis in the vascular wall in the other two groups. We even found a thrombus near the multi-tines expandable electrode needle insertion. The in vivo study data indicated the feasibility of a novel curved electrode for targeting tumors behind large vessels in the liver with reduced bleeding complications.

There were some limitations of our study. First, in this ex vivo study, we chose only one cross section from the gross pathology samples to indicate the ablation zone. The ablation volume of different electrodes should be systematically studied. Second, in the in vivo experiments, the ablations were conducted on normal canine hepatic tissue instead of on transplanted tumors behind the vessels. Due to the different tissue and tumor textures, the ablation range and cover effect would vary. Even so, the initial data from this animal model showed encouraging results of the new electrode in the tumor ablation field.

Conclusion

This study is a pilot study on the improvement of the RFA electrode design. The results have great clinical significance for the percutaneous ablation of tumors behind hepatic vessels by using RFA. The newly designed structure of the curved electrode could improve the accuracy of treating tumors with risky anatomic locations in the liver and protect the adjacent organ and vessels at the same time. Future preclinical studies are needed to evaluate the role of novel electrodes in the translation to clinical application.

Acknowledgements This study was supported by the National Natural Science Foundation of China (No. 81773286) and the Capital Characteristic Clinical Application Foundation (No. Z161100000516061).

Compliance with Ethical Standards

Conflict of interest The authors declare that they have no conflict of interest.

Ethical Standard All procedures performed in studies involving animals were in accordance with the ethical standards of the Institutional Animal Care and Use Committee (Peking University, Cancer Hospital). All applicable institutional guidelines for the care and use of animals were followed.

References

1. Ziemlewicz TJ, Wells SA, Lubner MG, Brace CL, Lee FT Jr, Hinshaw JL. Hepatic tumor ablation. Surg Clin North Am. 2016;96(2):315–39. https://doi.org/10.1016/j.suc.2015.12.006.
2. Decadt B, Siriwardena AK. Radiofrequency ablation of liver tumours: systematic review. Lancet Oncol. 2004;5(9):550–60. https://doi.org/10.1016/S1470-2045(04)01567-0.
3. Curley SA. Radiofrequency ablation of malignant liver tumors. Ann Surg Oncol. 2003;10(4):338–47. https://doi.org/10.1634/theoncologist.6-1-14.
4. Lencioni R, Crocetti L. Radiofrequency ablation of liver cancer. Tech Vasc Interv Radiol. 2007;10(1):38–46. https://doi.org/10.1053/j.tvir.2007.08.006.
5. Goldberg SN. Radiofrequency tumor ablation: principles and techniques. Eur J Ultrasound. 2001;13(2):129–47. https://doi.org/10.1016/S0929-8266(01)00126-4.
6. McWilliams JP, Yamamoto S, Raman SS, Loh CT, Lee EW, Liu DM, Kee ST. Percutaneous ablation of hepatocellular carcinoma: current status. J Vasc Interv Radiol. 2010;21(8 Suppl):S204–13. https://doi.org/10.1016/j.jvir.2009.11.025.
7. Ikeda K, Osaki Y, Nakanishi H, Nasu A, Kawamura Y, Jyoko K, Sano T, Sunagozaka H, Uchino K, Minami Y, Saito Y, Nagai K, Inokuchi R, Kokubu S, Kudo M. Recent progress in radiofrequency ablation therapy for hepatocellular carcinoma. Oncology. 2014;87(Suppl 1):73–7. https://doi.org/10.1159/000368148.
8. Ni Y, Mulier S, Miao Y, Michel L, Marchal G. A review of the general aspects of radiofrequency ablation. Abdom Imaging. 2005;30(4):381–400. https://doi.org/10.1007/s00261-004-0253-9.
9. Terraz S, Constantin C, Majno PE, Spahr L, Mentha G, Becker CD. Image-guided multipolar radiofrequency ablation of liver tumours: initial clinical results. Eur Radiol. 2007;17(9):2253e61. https://doi.org/10.1007/s00330-007-0626-x.
10. Lin SM, Lin CC, Chen WT, Chen YC, Hsu CW. Radiofrequency ablation for hepatocellular carcinoma: a prospective comparison of four radiofrequency devices. J Vasc Interv Radiol. 2007;18(9):1118–25. https://doi.org/10.1016/j.jvir.2007.06.010.
11. Fu JJ, Wang S, Yang W, Gong W, Jiang AN, Yan K, Chen MH. Protective and heat retention effects of thermo-sensitive basement membrane extract (matrigel) in hepatic radiofrequency ablation in an experimental animal study. Cardiovasc Intervent Radiol. 2017;40(7):1077–85. https://doi.org/10.1007/s00270-017-1617-1.
12. Lee JD, Lee JM, Kim SW, Kim CS, Mun WS. MR imaging-histopathologic correlation of radiofrequency thermal ablation lesion in a rabbit liver model: observation during acute and chronic stages. Korean J Radiol. 2001;2(3):151–8. https://doi.org/10.3348/kjr.2001.2.3.151.
13. Lee JM, Han JK, Lee JY, Kim SH, Choi JY, Lee MW, Choi SH, Eo H, Choi BI. Hepatic radiofrequency ablation using multiple probes: ex vivo and in vivo comparative studies of monopolar versus multipolar modes. Korean J Radiol. 2006;7(2):106–17. https://doi.org/10.3348/kjr.2006.7.2.106.
14. Yoon JH, Lee JM, Han JK, Choi BI. Dual switching monopolar radiofrequency ablation using a separable clustered electrode: comparison with consecutive and switching monopolar modes in ex vivo bovine livers. Korean J Radiol. 2013;14(3):403–11. https://doi.org/10.3348/kjr.2013.14.3.403.
15. Goldberg SN, Gazelle GS, Compton CC, Mueller PR, Tanabe KK. Treatment of intrahepatic malignancy with radiofrequency ablation: radiologic-pathologic correlation. Cancer. 2000;88(11):2452–63. https://doi.org/10.1002/1097-0142(20000601)88:11%3c2452:AID-CNCR5%3e3.0.CO;2-3.
16. Lee ES, Lee JM, Kim KW, Lee IJ, Han JK, Choi BI. Evaluation of the in vivo efficiency and safety of hepatic radiofrequency ablation using a 15-G Octopus® in pig liver. Korean J Radiol. 2013;14:194–201. https://doi.org/10.3348/kjr.2013.14.2.194.
17. Gao J, Wang SH, Ding XM, Sun WB, Li XL, Xin ZH, Ning CM, Guo SG. Radiofrequency ablation for single hepatocellular carcinoma 3 cm or less as first-line treatment. World J Gastroenterol. 2015;21(17):5287–94. https://doi.org/10.3748/wjg.v21.i17.5287.
18. Yan K, Chen MH, Yang W, Wang YB, Gao W, Hao CY, Xing BC, Huang XF. Radiofrequency ablation of hepatocellular carcinoma: long-term outcome and prognostic factors. Eur J Radiol. 2008;67(2):336–47. https://doi.org/10.1016/j.ejrad.2007.07.007.
19. Lee YH, Hsu CY, Chu CW, Liu PH, Hsia CY, Huang YH, Su CW, Chiou YY, Lin HC, Huo TI. Radiofrequency ablation is better than surgical resection in patients with hepatocellular carcinoma within the Milan criteria and preserved liver function: a retrospective study using propensity score analyses. J Clin Gastroenterol. 2015;49(3):242–9. https://doi.org/10.1097/MCG.0000000000000133.
20. Solbiati L, Ahmed M, Cova L, Ierace T, Brioschi M, Goldberg SN. Small liver colorectal metastases treated with percutaneous radiofrequency ablation: local response rate and long-term survival with up to 10-year follow-up. Radiology. 2012;265(3):958–68. https://doi.org/10.1148/radiol.12111851.
21. Rhim H, Lim HK, Kim YS, Choi D, Lee WJ. Radiofrequency ablation of hepatic tumors: lessons learned from 3000 procedures. J Gastroenterol Hepatol. 2008;23(10):1492–500. https://doi.org/10.1111/j.1440-1746.2008.05550.x.
22. Appelbaum L, Sosna J, Pearson R, Perez S, Nissenbaum Y, Mertyna P, Libson E, Goldberg SN. Algorithm optimization for multitined radiofrequency ablation: comparative study in ex vivo and in vivo bovine liver. Radiology. 2010;254(2):430–40. https://doi.org/10.1148/radiol.09090207.
23. Dupuy DE, Goldberg SN. Image-guided radiofrequency tumor ablation: challenges and opportunities–part II. J Vasc Interv Radiol. 2001;12(10):1135–48. https://doi.org/10.1016/S1051-0443(07)61670-4.
24. Stippel DL, Bangard C, Prenzel K, Yavuzyasar S, Fischer JH, Hölscher AH. Which parameters are needed for targeting a multitined radiofrequency device: an approach to a simple algorithm. Langenbecks Arch Surg. 2009;394(4):671–9. https://doi.org/10.1007/s00423-008-0306-6.
25. Cha J, Kim YS, Rhim H, Lim HK, Choi D, Lee MW. Radiofrequency ablation using a new type of internally cooled electrode with an adjustable active tip: an experimental study in ex vivo bovine and in vivo porcine livers. Eur J Radiol. 2011;77(3):516–21. https://doi.org/10.1016/j.ejrad.2009.09.011.
26. Ni Y, Miao Y, Mulier S, Yu J, Baert AL, Marchal G. A novel "cooled-wet" electrode for radiofrequency ablation. Eur Radiol. 2000;10(5):852–4. https://doi.org/10.1007/s003300051018.
27. Furse A, Miller BJ, McCann C, Kachura JR, Jewett MA, Sherar MD. Radiofrequency coil for the creation of large ablations: ex vivo and in vivo testing. J Vasc Interv Radiol. 2012;23(11):1522–8. https://doi.org/10.1016/j.jvir.2012.08.015.
28. Kim JH, Won HJ, Shin YM, Kim SH, Yoon HK, Sung KB, Kim PN. Medium-sized (3.1-5.0 cm) hepatocellular carcinoma:

transarterial chemoembolization plus radiofrequency ablation versus radiofrequency ablation alone. Ann Surg Oncol. 2011;18(6):1624–9. https://doi.org/10.1245/s10434-011-1673-8.
29. Zhu K, Huang J, Lai L, Huang W, Cai M, Zhou J, Guo Y, Chen J. Medium or large hepatocellular carcinoma: sorafenib combined with transarterial chemoembolization and radiofrequency ablation. Radiology. 2018;288(1):300–7. https://doi.org/10.1148/radiol.2018172028.
30. Yuan H, Liu F, Li X, Guan Y, Wang M. Transcatheter arterial chemoembolization combined with simultaneous DynaCT-guided radiofrequency ablation in the treatment of solitary large hepatocellular carcinoma. Radiol Med. 2018. https://doi.org/10.1007/s11547-018-0932-1.
31. Francica G, Meloni MF, Riccardi L, de Sio I, Terracciano F, Caturelli E, Iadevaia MD, Amoruso A, Roselli P, Chiang J, Scaglione M, Pompili M. Ablation treatment of primary and secondary liver tumors under contrast-enhanced ultrasound guidance in field practice of interventional ultrasound centers. A multicenter study. Eur J Radiol. 2018;105:96–101. https://doi.org/10.1016/j.ejrad.2018.05.030.
32. Noeren N, Nijkamp MW, Berendsen T, Govaert KM, van Kessel CS, Borel Rinkes IH, van Hillegersberg R. Multipolar radiofrequency ablation for colorectal liver metastases close to major hepatic vessels. Surgeon. 2015;13(2):77–82. https://doi.org/10.1016/j.surge.2013.11.013.
33. Haemmerich D, Wright AW, Mahvi DM, Lee FT Jr, Webster JG. Hepatic bipolar radiofrequency ablation creates coagulation zones close to blood vessels: a finite element study. Med Biol Eng Comput. 2003;41:317e23. https://doi.org/10.1007/BF02348437.
34. Lu DS, Raman SS, Limanond P, Aziz D, Economou J, Busuttil R, Sayre J. Influence of large peritumoral vessels on outcome of radiofrequency ablation of liver tumors. J Vasc Interv Radiol. 2003;14(10):1267–74. https://doi.org/10.1097/01.RVI.0000092666.72261.6B.
35. Ahmed M, Liu Z, Afzal KS, Weeks D, Lobo SM, Kruskal JB, Lenkinski RE, Goldberg SN. Radiofrequency ablation: effect of surrounding tissue composition on coagulation necrosis in a canine tumor model. Radiology. 2004;230(3):761–7. https://doi.org/10.1148/radiol.2303021801.